JACS
JOURNAL OF THE AMERICAN CHEMICAL SOCIETY

Subscriber access provided by ISTANBUL TEKNIK UNIV

Article

Trisphenalenyl-Based Neutral Radical Molecular Conductor

Sushanta K. Pal, Mikhail E. Itkis, Fook S. Tham, Robert W. Reed, Richard T. Oakley, and Robert C. Haddon

J. Am. Chem. Soc., **2008**, 130 (12), 3942-3951 • DOI: 10.1021/ja077771o

Downloaded from http://pubs.acs.org on February 8, 2009

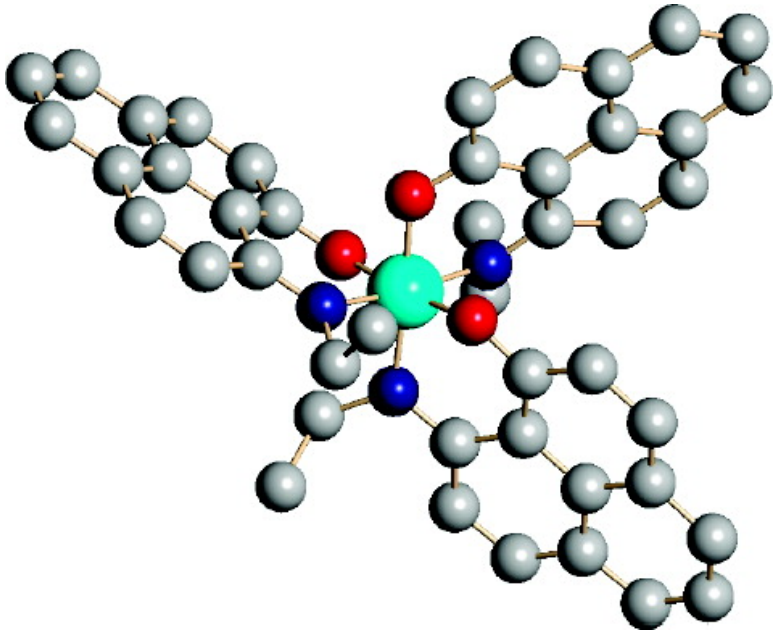

More About This Article

Additional resources and features associated with this article are available within the HTML version:

- Supporting Information
- Links to the 1 articles that cite this article, as of the time of this article download
- Access to high resolution figures
- Links to articles and content related to this article
- Copyright permission to reproduce figures and/or text from this article

View the Full Text HTML

ACS Publications
High quality. High impact.

Journal of the American Chemical Society is published by the American Chemical Society. 1155 Sixteenth Street N.W., Washington, DC 20036

J|A|C|S
ARTICLES
Published on Web 02/29/2008

Trisphenalenyl-Based Neutral Radical Molecular Conductor

Sushanta K. Pal,[†] Mikhail E. Itkis,[†] Fook S. Tham,[†] Robert W. Reed,[‡] Richard T. Oakley,[‡] and Robert C. Haddon*[,†]

Departments of Chemistry and Chemical & Environmental Engineering, University of California, Riverside, California 92521-0403, and Department of Chemistry, University of Waterloo, Waterloo, Ontario N2L 3G1, Canada

Received October 9, 2007; E-mail: haddon@ucr.edu

Abstract: We report the preparation, crystallization, and solid-state characterization of the first member of a new family of tris(1,9-disubstituted phenalenyl)silicon neutral radicals. In the solid state, the radical packs as weak partial π-dimers with intermolecular carbon···carbon contacts that fall at the van der Waals atomic separation. Magnetic susceptibility measurements indicate ~0.7 Curie spins per molecule from room temperature down to 50 K, below which antiferromagnetic coupling becomes apparent; the compound has a room-temperature single-crystal conductivity of $\sigma_{RT} = 2.4 \times 10^{-6}$ S cm^{-1}.

Introduction

The concept of using neutral radicals as building blocks for molecular conductors provides an alternative approach to the conventional charge-transfer organic conductors and superconductors, in which the unpaired electrons of the neutral radicals serve as charge carriers.[1−3] The idea of using the phenalenyl system as a building block for designing intrinsic molecular conductors and superconductors is not only appealing but also challenging, and this system has attracted theoretical and experimental attention.[4−11]

Phenalenyl is a well-known odd alternate hydrocarbon with high symmetry (D_{3h}) which has the ability to form three redox species: cation, radical, and anion.[12−14] Such characteristic features have been widely utilized for exploring new conjugated organic electronic and magnetic materials,[15] and some of the phenalenyl radicals undergo dimerization either by π-association or by σ-association. Recent progress in phenalenyl chemistry[4−8,9,16−19] has led to the isolation of the radical itself in the crystalline state through the introduction of substituents.[4,5,7]

There are a number of difficulties in the realization of a molecular metal based on phenalenyl: (1) the strength of the carbon···carbon bond makes it difficult to suppress σ-dimerization, (2) like most delocalized organic radicals, phenalenyl is planar and therefore predisposed to the formation of one-dimensional stacks that are subject to electronic instabilities with insulating ground states, and (3) radicals are usually expected to give rise to exactly half-filled bands, which lead to Mott insulators because of the large on-site Coulombic correlation energy.

Because of the considerations enumerated above, we felt it was important to attempt to design molecules that avoided the problems associated with an exactly half-filled band and also circumvented the one-dimensionality that is characteristic of many planar conjugated π-systems, and this led us to crystallize a series of spiro-biphenalenyl radicals that overcome most of these objections and have led to unique solid-state properties (Scheme 1, **1**−**15**).[20−29]

Because the spiro-biphenalenyl radicals are composed of two phenalenyl systems that are held perpendicular, the usual

[†] University of California, Riverside.
[‡] University of Waterloo.

(1) Haddon, R. C. *Nature* **1975**, *256*, 394−396.
(2) Haddon, R. C. *Aust. J. Chem.* **1975**, *28*, 2343−2351.
(3) Oakley, R. T. *Can. J. Chem.* **1993**, *71*, 1775−1784.
(4) Goto, K.; Kubo, T.; Yamamoto, K.; Nakasuji, K.; Sato, K.; Shiomi, D.; Takui, T.; Kubota, M.; Kobayashi, T.; Yakusi, K.; Ouyang, J. *J. Am. Chem. Soc.* **1999**, *121*, 1619−1620.
(5) Morita, Y.; Aoki, T.; Fukui, K.; Nakazawa, S.; Tamaki, K.; Suzuki, S.; Fuyuhiro, A.; Yamamoto, K.; Sato, K.; Shiomi, D.; Naito, A.; Takui, T.; Nakasuji, K. *Angew. Chem., Int. Ed.* **2002**, *41*, 1793−1796.
(6) Fukui, K.; Sato, K.; Shiomi, D.; Takui, T.; Itoh, K.; Gotoh, K.; Kubo, T.; Yamamoto, K.; Nakasuji, K.; Naito, A. *Synth. Met.* **1999**, *103*, 2257−2258.
(7) Koutentis, P. A.; Chen, Y.; Cao, Y.; Best, T. P.; Itkis, M. E.; Beer, L.; Oakley, R. T.; Brock, C. P.; Haddon, R. C. *J. Am. Chem. Soc.* **2001**, *123*, 3864−3871.
(8) Takano, Y.; Taniguchi, T.; Isobe, H.; Kubo, T.; Morita, Y.; Yamamoto, K.; Nakasuji, K.; Takui, T.; Yamaguchi, K. *J. Am. Chem. Soc.* **2002**, *124*, 11122−11130.
(9) Takano, Y.; Taniguchi, T.; Isobe, H.; Kubo, T.; Morita, Y.; Yamamoto, K.; Nakasuji, K.; Takui, T.; Yamaguchi, K. *Chem. Phys. Lett.* **2002**, *358*, 17−23.
(10) Huang, J.; Kertesz, M. *J. Am. Chem. Soc.* **2006**, *128*, 1418−1419.
(11) Huang, J.; Kertesz, M. *J. Am. Chem. Soc.* **2006**, *128*, 7277−7286.
(12) Reid, D. H. *Q. Rev., Chem. Soc.* **1965**, *19*, 274−302.
(13) Reid, D. H. *Chem. Ind.* **1956**, 1504−1505.
(14) Reid, D. H. *Tetrahedron* **1958**, *3*, 339−352.
(15) Itkis, M. E.; Chi, X.; Cordes, A. W.; Haddon, R. C. *Science* **2002**, *296*, 1443−1445.
(16) Small, D.; Zaitsev, V.; Jung, Y.; Rosokha, S. V.; Head-Gordon, M.; Kochi, J. K. *J. Am. Chem. Soc.* **2004**, *126*, 13850−13858.
(17) Zheng, S.; Lan, J.; Khan, S. I.; Rubin, Y. *J. Am. Chem. Soc.* **2003**, *125*, 5786−5791.
(18) Zheng, S.; Thompson, J. D.; Tontcheva, A.; Khan, S. I.; Rubin, Y. *Org. Lett.* **2005**, *7*, 1861−1863.
(19) Kubo, T.; Shimizu, A.; Sakamoto, M.; Uruichi, M.; Yakushi, K.; Nakano, M.; Shiomi, D.; Sato, K.; Takui, T.; Morita, Y.; Nakasuji, K. *Angew. Chem., Int. Ed.* **2005**, *44*, 6564−6568.
(20) Chi, X.; Itkis, M. E.; Patrick, B. O.; Barclay, T. M.; Reed, R. W.; Oakley, R. T.; Cordes, A. W.; Haddon, R. C. *J. Am. Chem. Soc.* **1999**, *121*, 10395−10402.
(21) Chi, X.; Itkis, M. E.; Kirschbaum, K.; Pinkerton, A. A.; Oakley, R. T.; Cordes, A. W.; Haddon, R. C. *J. Am. Chem. Soc.* **2001**, *123*, 4041−4048.
(22) Chi, X.; Itkis, M. E.; Reed, R. W.; Oakley, R. T.; Cordes, A. W.; Haddon, R. C. *J. Phys. Chem. B* **2002**, *106*, 8278−8287.
(23) Chi, X.; Itkis, M. E.; Tham, F. S.; Oakley, R. T.; Cordes, A. W.; Haddon, R. C. *Int. J. Quantum Chem.* **2003**, *95*, 853−865.

 10.1021/ja077771o CCC: $40.75 **© 2008 American Chemical Society**

Scheme 1

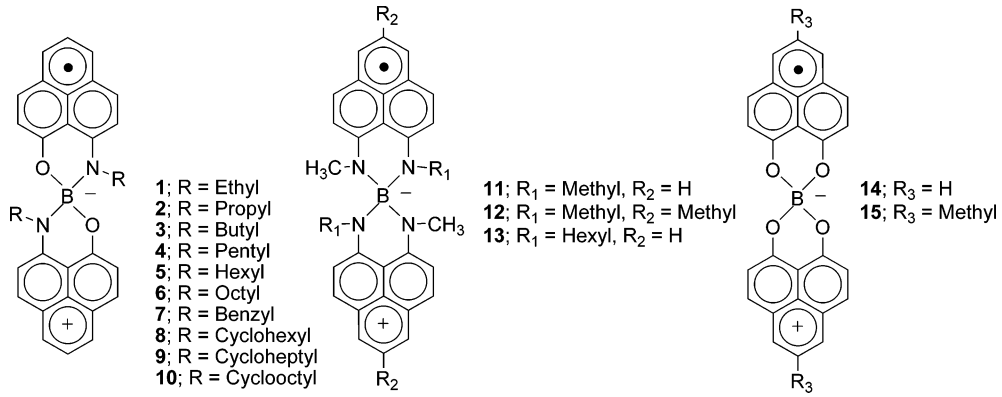

Scheme 2

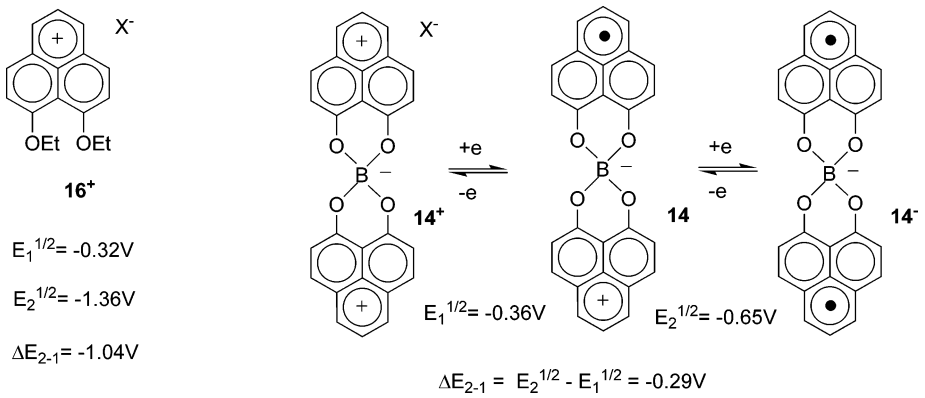

Table 1. Half-Wave Potentials and Disproportionation Potentials (Volts vs SCE) for Phenalenyl Complex Salts in Acetonitrile

salt		$E_1^{1/2}$	$E_2^{1/2}$	$E_3^{1/2}$	ΔE_{2-1}
16$^+$$PF_6^-$	1PLY	−0.32	−1.36		−1.04
1$^+$$BPh_4^-$	B, 2PLY	−0.75	−1.10		−0.35
12$^+$$BPh_4^-$	B, 2PLY	−1.06	−1.41		−0.35
14$^+$TFPB$^-$	B, 2PLY	−0.36	−0.65		−0.29
17$^+$TFPB$^-$	Si, 3PLY	−0.57	−0.81	−1.13	−0.24
18$^+$TFPB$^-$	Ge, 3PLY	−0.56	−0.78	−1.06	−0.22
19$^+$$BPh_4^-$	Si, 3PLY	−0.97	−1.19	−1.43	−0.22
20$^+$$BPh_4^-$	Si, 3PLY	−0.89	−1.24	−1.49	−0.35

1-D superimposed π-stacking arrangement is inhibited and the electronic structure is such that crystallization of the radical will lead to a one-quarter-filled band in the solid state, thereby minimizing the on-site Coulombic correlation energy associated with a charge fluctuation.[30] This latter point is illustrated in Scheme 2, where it may be seen that the availability of two distinct sites of reduction in the same molecule considerably reduces the disproportionation potential ($|\Delta E_{2-1}|$).[30]

In the present article, we explore an extension of this strategy in which we incorporate three phenalenyl systems into the same molecule; this approach is designed to produce a one-sixth-filled band in the solid state while still inhibiting the formation of the usual 1-D superimposed π-stacking arrangement.

Trisphenalenyls. We have previously reported the synthesis and solution properties of cationic propeller-shaped 9-oxidophenalenone complexes of silicon(IV)[**17**$^+$TFPB$^-$] and germanium(IV) containing three phenalenyl units in the same molecule that are oriented in an octahedral geometry,[31] and a silicon(IV) salt based on a new redox active tripodal hexadentate ligand [H_3L = 1,1,1-tris(1′-oxophenalenyl-9′-*N*-methyl)ethane].[32]

As may be seen in Scheme 3, a number of valence representations are possible for these compounds, but the electrochemistry supports the idea that the 9-oxidophenalenone unit bears most of the positive charge (Schemes 4 and 5). The cyclic voltammograms of **17**$^+$TFPB$^-$, **18**$^+$TFPB$^-$, and **19**$^+$$BPh_4^-$ show three reversible one-electron reduction steps due to the formation of radical, anion, and dianion as each phenalenyl moiety accepts an electron; the cyclic voltammetry measurements and disproportionation potentials are listed in Table 1.

The redox chemistry of this class of compounds is a strong function of the number of phenalenyl units (PLY) that are incorporated into a single molecule, as illustrated by the oxygen-substituted compounds **16**$^+$, **14**$^+$, and **17**$^+$ that contain one, two, and three PLY units per molecule, respectively. First, it may be seen that the ease of first reduction follows the sequence

(24) Pal, S. K.; Itkis, M. E.; Reed, R. W.; Oakley, R. T.; Cordes, A. W.; Tham, F. S.; Siegrist, T.; Haddon, R. C. *J. Am. Chem. Soc.* **2004**, *126*, 1478−1484.
(25) Liao, P.; Itkis, M. E.; Oakley, R. T.; Tham, F. S.; Haddon, R. C. *J. Am. Chem. Soc.* **2004**, *126*, 14297−14302.
(26) Mandal, S. K.; Itkis, M. E.; Chi, X.; Samanta, S.; Lidsky, D.; Reed, R. W.; Oakley, R. T.; Tham, F. S.; Haddon, R. C. *J. Am. Chem. Soc.* **2005**, *127*, 8185−8196.
(27) Pal, S. K.; Itkis, M. E.; Tham, F. S.; Reed, R. W.; Oakley, R. T.; Haddon, R. C. *Science* **2005**, *309*, 281−284.
(28) Mandal, S. K.; Samanta, S.; Itkis, M. E.; Jensen, D. W.; Reed, R. W.; Oakley, R. T.; Tham, F. S.; Donnadieu, B.; Haddon, R. C. *J. Am. Chem. Soc.* **2006**, *128*, 1982−1994.
(29) Pal, S. K.; Itkis, M. E.; Tham, F. S.; Reed, R. W.; Oakley, R. T.; Donnadieu, B.; Haddon, R. C. *J. Am. Chem. Soc.* **2007**, *129*, 7163−7174.
(30) Haddon, R. C.; Chichester, S. V.; Marshall, J. H. *Tetrahedron* **1986**, *42*, 6293−6300.
(31) Pal, S. K.; Tham, F. S.; Reed, R. W.; Oakley, R. T.; Haddon, R. C. *Polyhedron* **2005**, *24*, 2076−2083.
(32) Samanta, S.; Itkis, M. E.; Reed, R. W.; Oakley, R. T.; Tham, F. S.; Haddon, R. C. *Synth. Met.* **2005**, *154*, 285−288.

Scheme 3

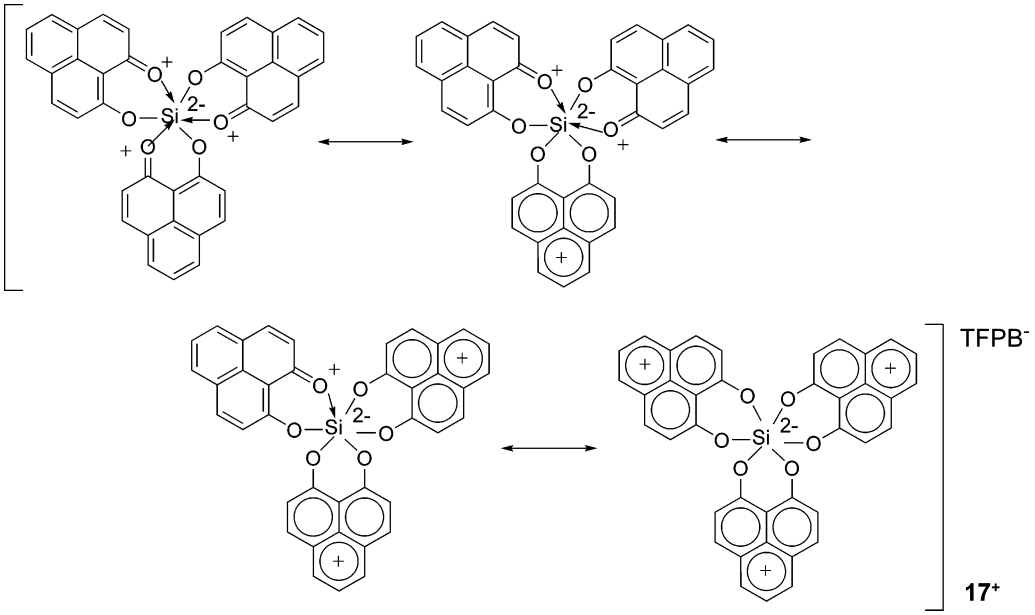

Scheme 4

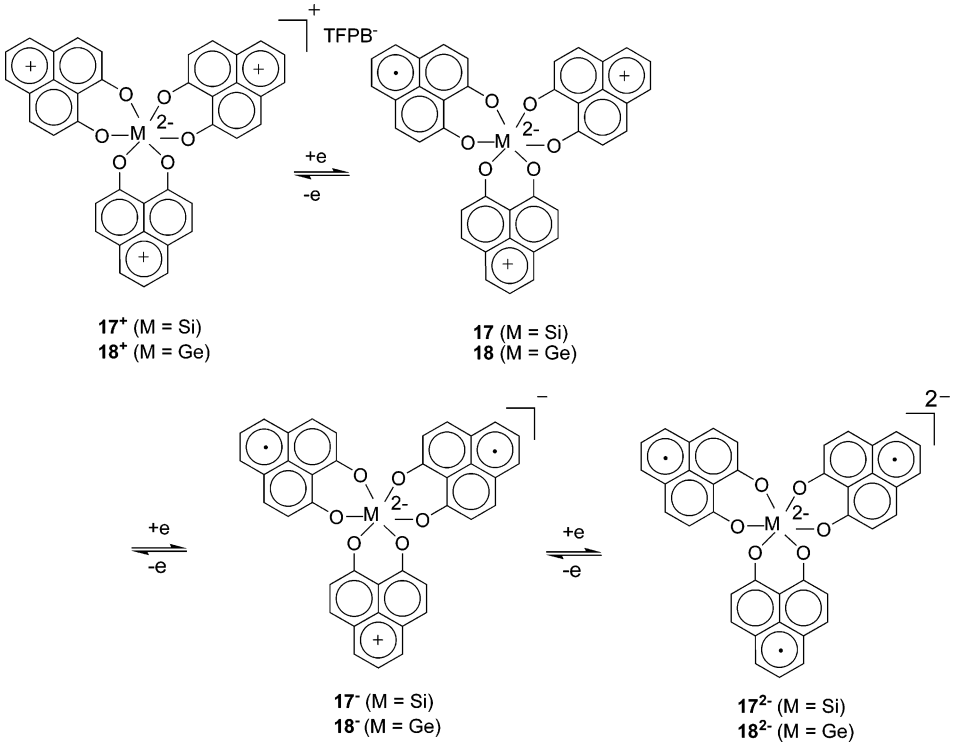

16$^+$ (1 PLY, $E_1^{1/2} = -0.32$ V), **14**$^+$ (2 PLY, $E_1^{1/2} = -0.36$ V), and **17**$^+$ (3 PLY, $E_1^{1/2} = -0.57$ V). One factor that influences this sequence may be understood by considering the degree of charge that is localized on a single phenalenyl ring system in the complexes: clearly one phenalenyl ring bears most of the charge density in the salt containing one phenalenyl unit, and within this series it is apparent that any given phenalenyl unit will bear a lower positive charge as the number of the phenalenyl units increases, and therefore, the first electron transfer becomes progressively more difficult. Of more importance in the present context is the trend in the disproportionation potentials (ΔE_{2-1}), where it may be seen that the absolute values decrease as the number of sites of reduction increases: **16**$^+$ (1 PLY, $\Delta E_{2-1} = -1.04$ V), **14**$^+$ (2 PLY, $\Delta E_{2-1} = -0.29$ V), and **17**$^+$ (3 PLY, $\Delta E_{2-1} = -0.24$ V), and it for this reason that we have pursued the trisphenalenyl radicals for a number of years.[31,32] The position of the first and second reduction waves in the cyclic voltammetry depends on the nature of the heteroatoms (X, Y) attached to the disubstituted -phenalenyl system, and the first reduction potential moves to more positive values along the series (X, Y) = (N, N); (N, O); (O, O).

Results and Discussion

Preparation and Solution Properties of Radical (20). In the present article, we focus on an amino derivative of the trisphenalenyl compound, because this compound was the first

Scheme 5

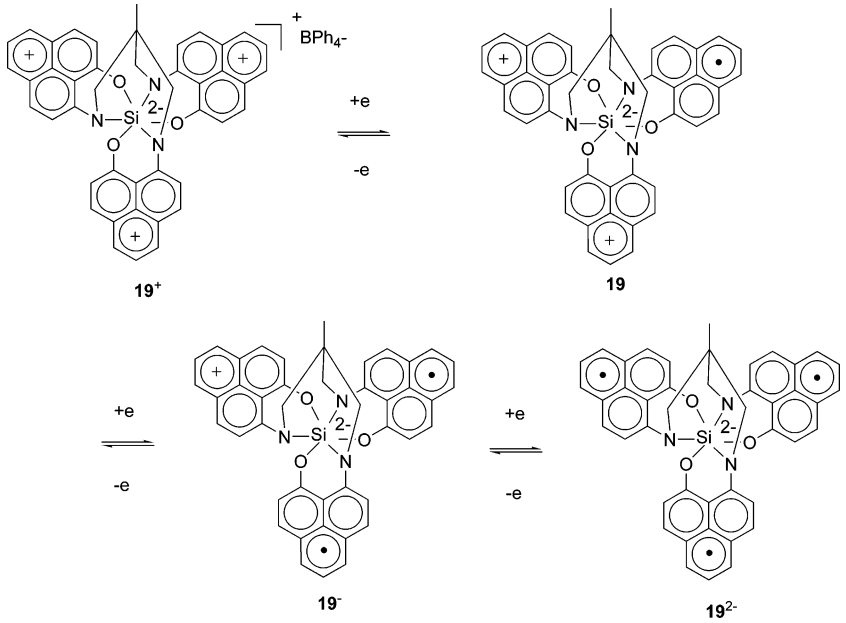

Scheme 6

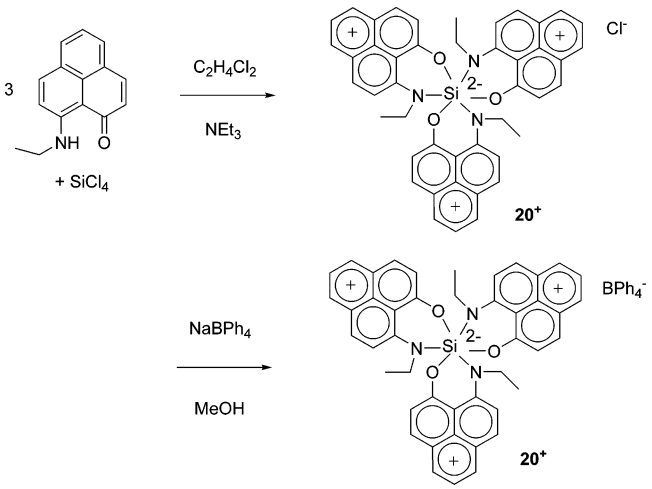

in this series to give rise to high-quality crystals of the radical that were suitable for complete solid-state characterization. We first prepared the chloride salt ($\mathbf{20}^+Cl^-$) and then exchanged the counterion for the tetraphenylborate (BPh_4^-) anion to purify the salt and to achieve the required solubility properties (Scheme 6). The compound $\mathbf{20}^+BPh_4^-$ was purified by recrystallization from acetonitrile to give material suitable for radical preparation and crystal growth.

The electrochemistry of $\mathbf{20}^+BPh_4^-$ is presented in Figure 1. It may be seen that the compound shows three reversible redox waves (Scheme 4), but the first reduction occurs more easily than that in the case of $\mathbf{19}^+TFPB^-$. Furthermore, the disproportionation potential of $\mathbf{20}^+$, $\Delta E_{2-1} = E_2^{1/2} - E_1^{1/2} = -0.35$ V, is considerably higher in magnitude than the values found for the other trisPLY compounds ($\mathbf{17}^+-\mathbf{19}^+$) and is comparable to the ΔE_{2-1} values found for spiro-bis(1,9-diamino-substituted phenalenyl)boron compounds which contain two PLY units.[28]

After a number of attempts to crystallize **20**, we found that the direct mixing of a chemical reductant with the precursor salt in a glass vial gave reproducible yields (~60%) of high-quality, long, black needles of the radical. We used cobaltocene as reductant because the oxidation potential ($E^{1/2} = -0.91$ V)[33] of cobaltocene falls between the $E_1^{1/2}$ and $E_2^{1/2}$ reduction potentials of $\mathbf{20}^+BPh_4^-$ (Scheme 7). After the two solutions were physically mixed, the glass vial was sealed and carefully removed from the glove box; crystal nucleation started overnight, and the crystals reach their optimum size and quality in 4−6 days.

Though solutions of the radical **20** are extremely oxygen-sensitive, the crystals are stable enough to allow chemical analysis, X-ray crystal structure characterization, and other solid-state measurements.

X-ray Crystal Structure of 20. The X-ray crystal structure of **20** was determined at two different temperatures (100 K and room temperature, $T = 293$ K) to test for the presence of phase transitions, such as those observed in the case of boron compounds reported previously.[21] The crystal data are summarized in Table 2 and Figure 2a shows an ORTEP drawing of the molecule together with the atom numbering. The most important point for our purposes is the absence of simple σ-dimerization, even though we did not employ bulky substituents at the active position of the phenalenyl nucleus to suppress intermolecular carbon···carbon bond formation.[7,34,35] Carbon-based free radicals usually require steric hindrance to suppress σ-dimerization in the solid state,[4,36] and we are not aware of any other system where resonance stabilization has been sufficient to allow the realization of carbon-based free radicals in the solid state. The asymmetric unit of molecule **20** consists of the complete molecule, and the distinctive feature of the phenalenyl packing is a weak π-dimer with a separation between phenalenyl rings of 3.39 Å.

The presence of three unsymmetrical bidentate ligands in an octahedral geometry gives rise to the possibility of facial and meridional geometrical isomers; we isolated crystalline **20** as

(33) Robbins, J. L.; Edelstein, N.; Spencer, B.; Smart, J. C. *J. Am. Chem. Soc.* **1982**, *104*, 1882−1893.
(34) Haddon, R. C.; Wudl, F.; Kaplan, M. L.; Marshall, J. H.; Cais, R. E.; Bramwell, F. B. *J. Am. Chem. Soc.* **1978**, *100*, 7629−7633.
(35) Haddon, R. C.; Chichester, S. V.; Stein, S. M.; Marshall, J. H.; Mujsce, A. M. *J. Org. Chem.* **1987**, *52*, 711−712.
(36) Griller, D.; Ingold, K. U. *Acc. Chem. Res.* **1976**, *9*, 13−19.

Scheme 7

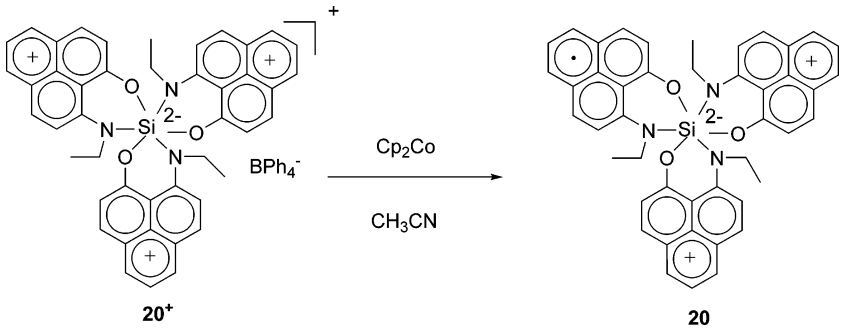

Table 2. Crystal Data for Radical **20**

formula		$C_{45}H_{36}N_3O_3Si$	
fw		694.86	
crystal system		monoclinic	
space group		*P*2(1)/*n*	
temp (K)	100(2)		293(2)
a, Å	11.3316(10)		11.4019(16)
b, Å	14.4199(13)		14.563(2)
c, Å	21.2689(19)		21.455(3)
V, Å^3	3402.0(5)		3483.3(8)
α, deg	90		90
β, deg	101.7890(10)		102.095(2)
γ, deg	90		90
θ range, deg	1.72−28.28		1.70−23.26
indep. reflns	8453		5014
final *R* indices	R1 = 0.0543		R1 = 0.0481
[$I > 2\sigma(I)$]	wR2 = 0.1357		wR2 = 0.1179
R indices	R1 = 0.0914		R1 = 0.0818
(all data)	wR2 = 0.1568		wR2 = 0.1396
mean plane separation, Å	3.39		3.46

the meridional isomer, and we did not observe the facial isomer during crystallization (Figure 3).The molecular geometry around silicon consists of three bidentate chelating phenalenyl ligands (labeled PLY1, PLY2, and PLY3; Figure 2), and the coordination of the oxygen and nitrogen atoms around silicon is nearly octahedral. However, the structure of **20** is strongly distorted because of bending of the phenalenyl units; all three of the phenalenyl units in **20** undergo severe bending at the heteroatoms (O and N) attached to silicon, with bending angles of 26° (PLY1), 34° (PLY2), and 30° (PLY3); the analogous bending angles for the cation (**20**$^+$BPh$_4^-$) are 24°, 40°, and 38°, respectively.

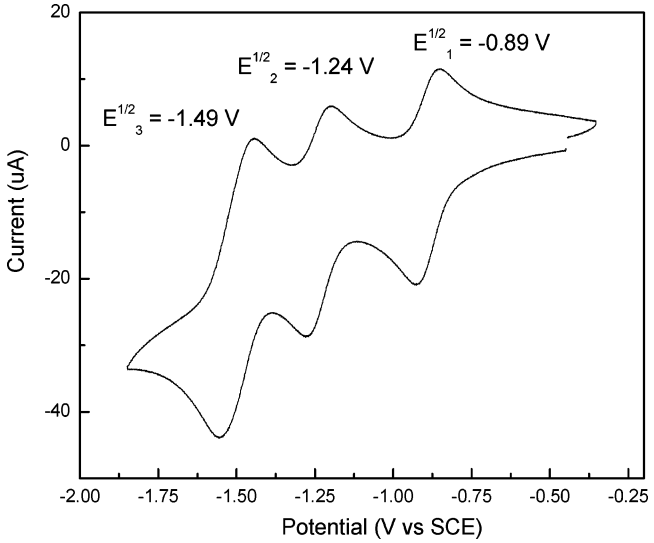

Figure 1. Cyclic voltammetry of **20**$^+$BPh$_4^-$ in acetonitrile, reference to SCE via internal ferrocene (not shown).

The radical **20** exists as a partial *π*-dimer (Figure 4), with mean separations between the molecular planes of 3.39 Å (T = 100 K) and 3.46 Å (T = 293 K), which fall right at the expected van der Waals distance between pairs of carbon atoms (3.4 Å). These interatomic distances may be compared with the mean plane separations seen in the ethyl radical (**1**): 3.18 Å (T = 100 K, diamagnetic) and 3.31 Å (T = 173 K, paramagnetic), and delocalized Pauli paramagnetic radicals **8**: 3.28 Å (T = 223 K), **9**: 3.26 Å (T = 100 K), **14**: 3.17 Å (100 K) and 3.22 Å (293 K). The projection given in Figure 5 shows that the *π*-dimerization is far from optimal with only two pairs of the six active carbon atoms with large spin density involved in direct contact, together with two other contacts involving the central atom of the phenalenyl ring which is known to possess a small negative spin density.[28] The closest individual carbon···carbon distances are 3.40, 3.42 Å (Figure 5) at 100 K and 3.48, 3.49 Å at 293 K, which are close to the van der Waals separation for carbon atoms, but significantly longer than the values seen in Pauli paramagnetic radicals such as **9** (3.27−3.36 Å), and much longer than the values in diamagnetic radicals such as **1**; thus, it is clear that this *π*-dimer is much weaker than other systems isolated to date.

The packing of the molecules in *y*- and *z*-directions is shown in Figure 4, and it is apparent that the molecules exist as individual *π*-dimers, and the closest carbon···carbon distances between dimers are 3.49 Å. The packing in the *x*-direction is quite different from the packing in the *y*- and *z*-directions. The molecules form a stack along the *x*-axis (Figure 6a), and the closest carbon···carbon distances between molecules along this direction are 3.60 and 3.94 Å (spin-bearing carbon atom), together with the partial *π*-dimer interactions of 3.40 and 3.42 Å (Figure 6b).

Thus, it is apparent that the structure of the radical **20** is severely distorted by the crystal packing, although there is a symmetry breaking that is largely intramolecular in origin. The bond lengths around silicon are irregular with Si−N bond lengths of 1.92 (PLY1), 1.91 (PLY2), and 1.83 Å (PLY3), and Si−O bond lengths of 1.76 (PLY1), 1.78 (PLY2), and 1.72 Å (PLY3); the shorter bond distances to silicon observed for PLY3 suggest that there is higher electron density on this unit, and thus this is the primary site of the unpaired electron. On the basis of previous work,[15,37] the localization of the spin density is also associated with bond length variations in the phenalenyl

(37) Chi, X.; Tham, F. S.; Cordes, A. W.; Itkis, M. E.; Haddon, R. C. *Synth. Met.* **2003**, *133*−*134*, 367−372.

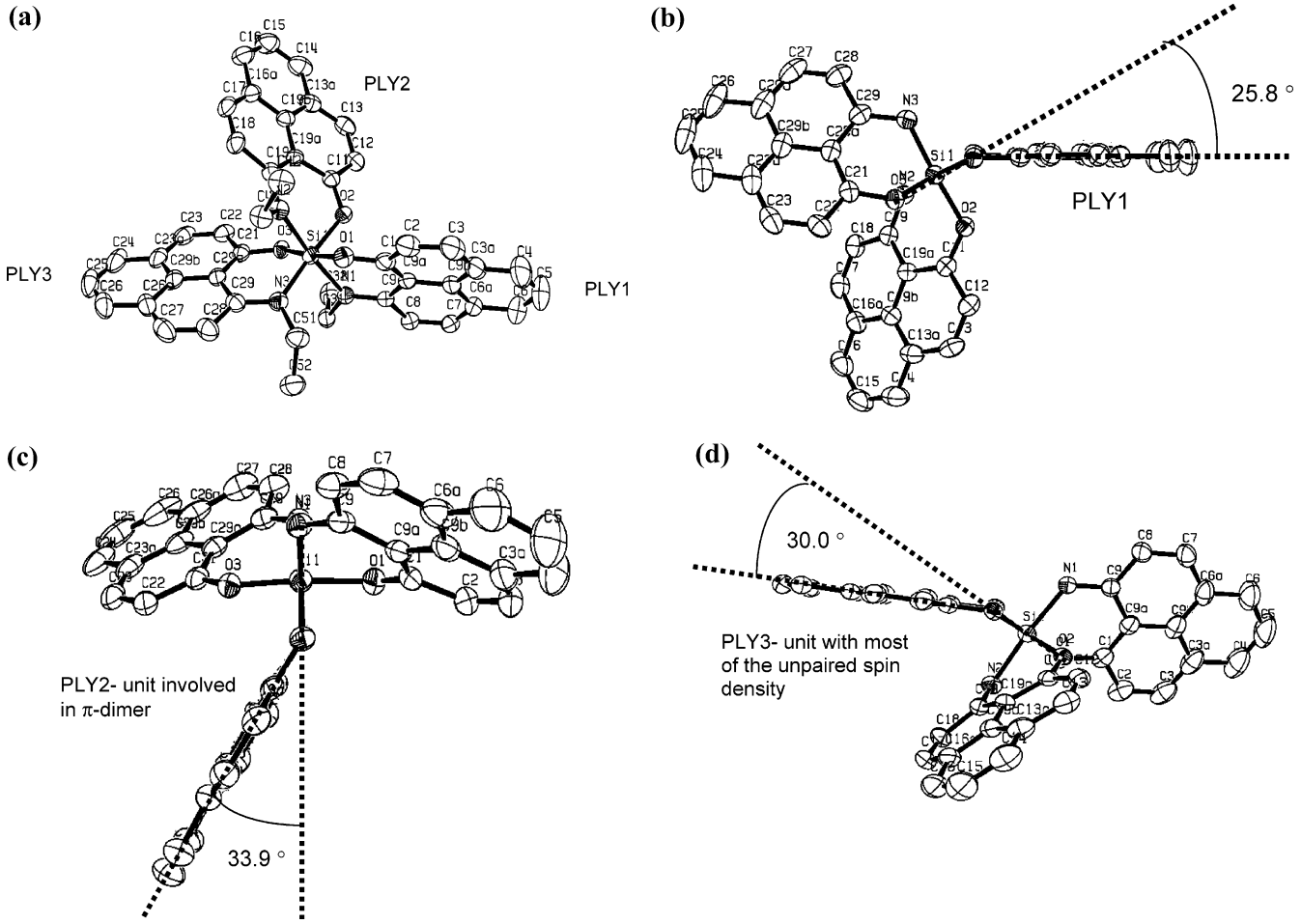

Figure 2. ORTEP diagram of **20** (at 100 K). All of the phenalenyl units in **20** undergo severe bending (25.8°, 33.9°, and 30°) at the heteroatoms (O and N) attached to silicon.

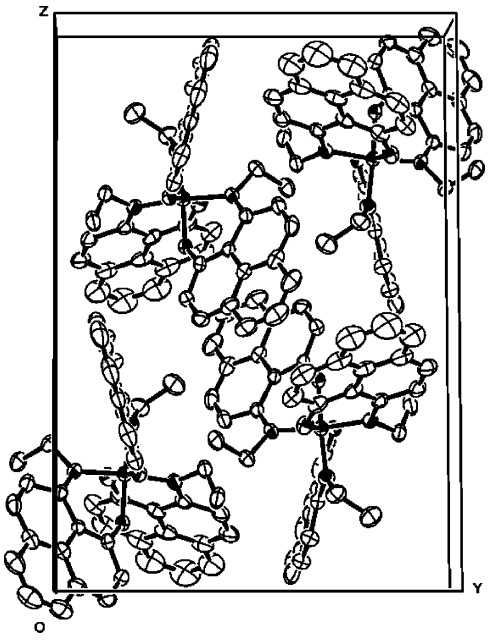

Figure 3. Unit cell of crystalline **20** viewed down the *x*-axis.

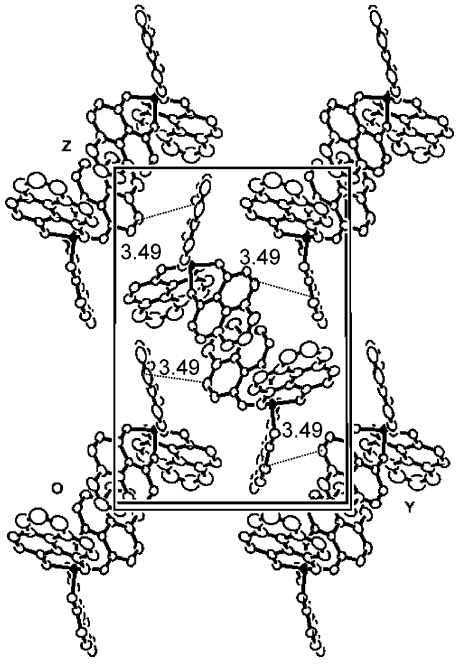

Figure 4. Packing of the molecules and closest intermolecular contacts between phenalenyl units in the crystal lattice of **20**, with ethyl groups omitted.

units, and in an effort to seek further information on this point we calculated the standard deviations of the bond lengths in each phenalenyl unit of **20** with reference to the bond lengths in the cation ($\mathbf{20}^{+}BPh_4^{-}$). From the bond length and standard deviation calculation (Table S10, Supporting Information), we conclude that the unpaired spin is primarily located on the PLY3

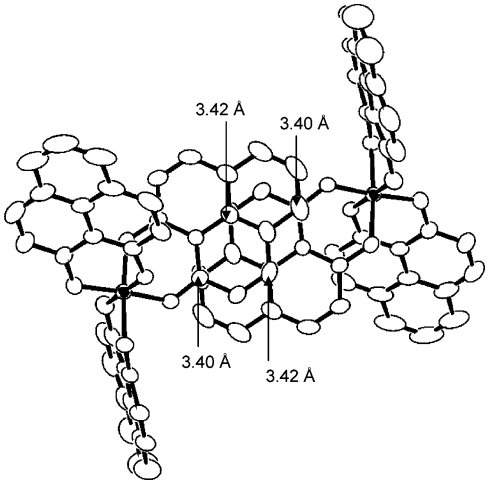

Figure 5. Slipped, partial π-dimer structure of crystalline **20** at $T = 100$ K, with ethyl groups omitted.

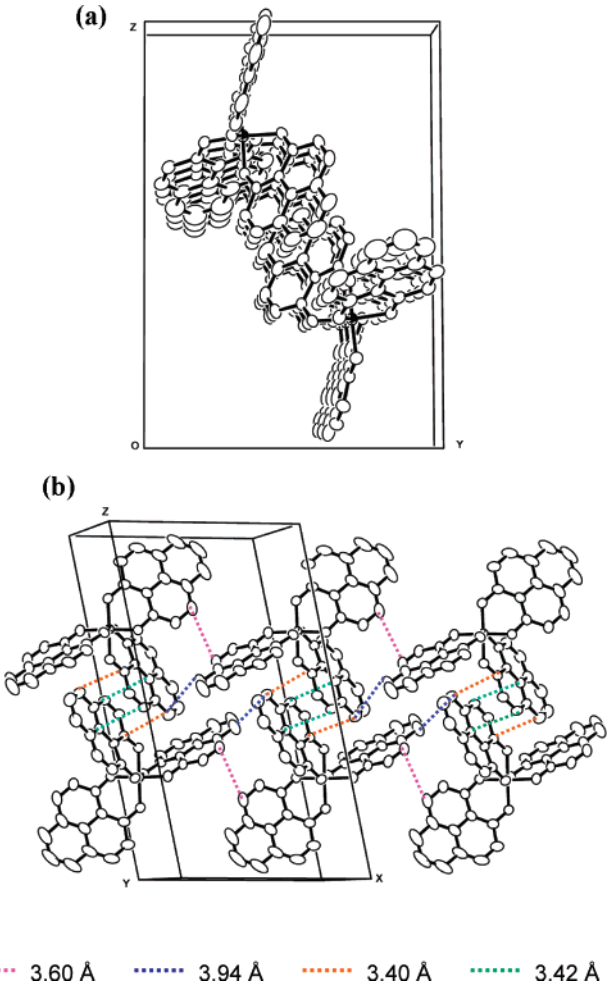

Figure 6. Packing of **20** along the *x*-axis. (a) Viewed along *x*-axis and (b) showing close contacts along the *x*-axis, with ethyl groups omitted.

phenalenyl ring with carbon numbering C (21) to C (29b) (Figure 2). Thus, the spin-bearing phenalenyl ring (PLY3) does not participate in the partial π-dimer formation, whereas the PLY2 phenalenyl ring (carbon numbering C (11) to C (19b)), which is involved in the partial π-dimer formation in the crystal lattice, does not show evidence for spin localization, at least at the accessible temperatures for structural determination. Given

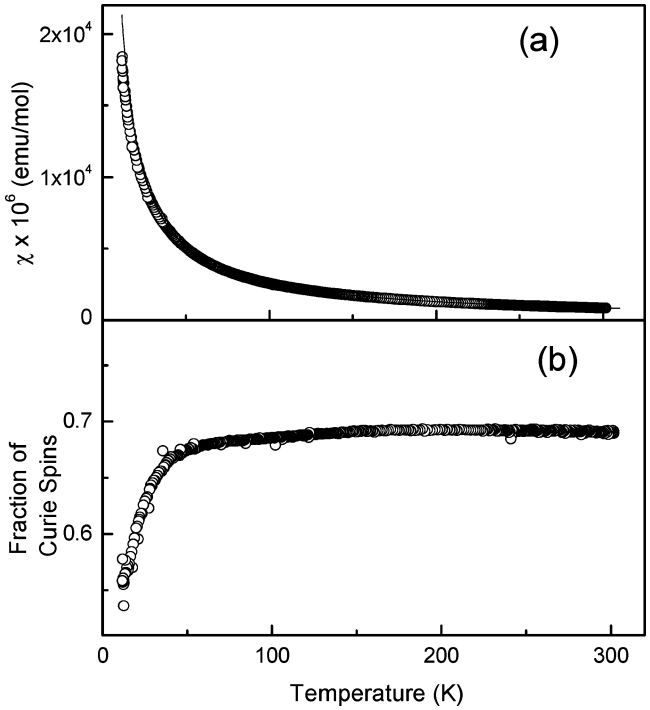

Figure 7. (a) Magnetic susceptibility of crystalline **20** as function of temperature. The solid line is a Curie−Weiss fit to the data. (b) Fraction of effective Curie spins per molecule versus temperature.

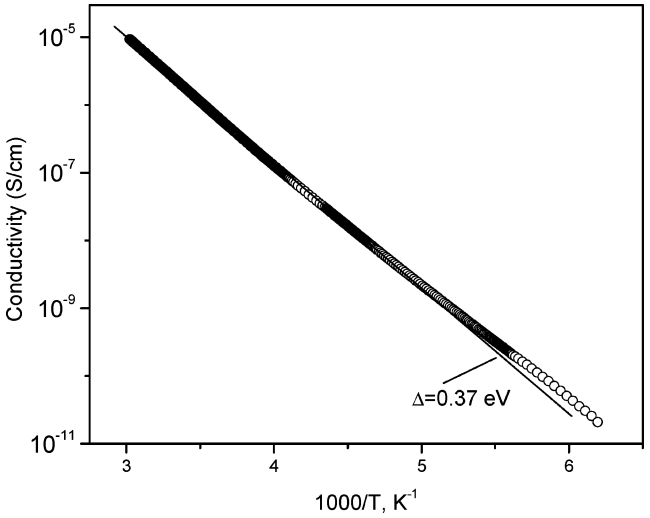

Figure 8. Single-crystal conductivity of **20** as a function of temperature.

the large interplanar separation and poor orbital overlap which are apparent in the partial π-dimer (above), it is not surprising that this phenalenyl unit does not serve as the location of the unpaired electron, although this may not be the case at low temperatures (below).

Magnetic Susceptibility and Conductivity. We measured the magnetic susceptibility (χ) of **20** over the temperature range 10−300 K using a Faraday balance. The compound shows Curie−Weiss magnetic behavior, and by fitting the experimental data to the Curie−Weiss function $\chi = \chi_0 + C/(T + \theta)$, we obtain a Curie constant, $C = 0.26$ emu*K/mol, $\theta = 0.75$ K, corresponding to a weak antiferromagnetic interaction. The diamagnetic core contribution $\chi_0 = -423 \times 10^{-6}$ emu/mol was calculated utilizing published values for the Pascal constants (Supporting Information).

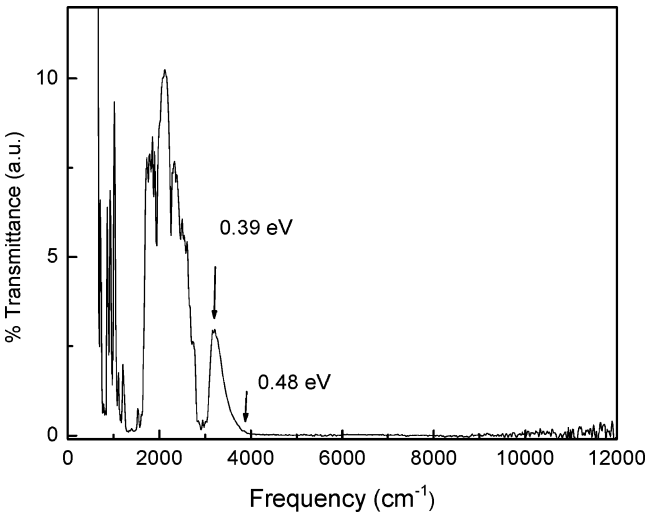

Figure 9. Single-crystal IR and UV−visible transmission spectrum of crystalline **20**.

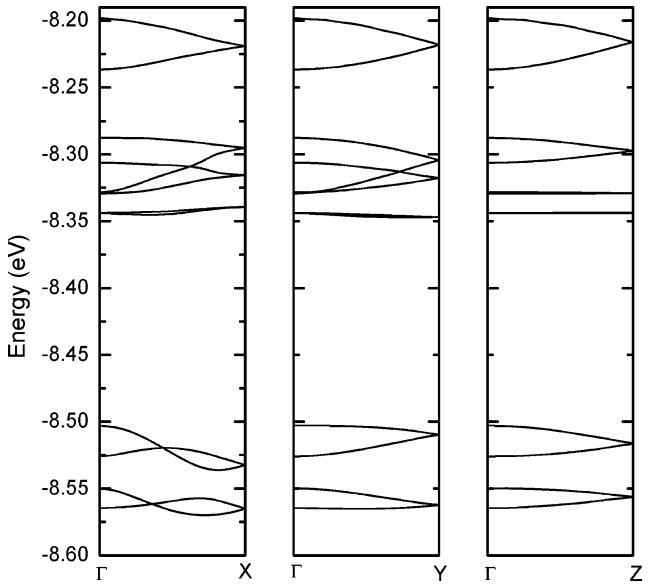

Figure 10. EHT band structure calculated for the experimental structure of crystalline **20**.

The Curie constant obtained above is significantly below the value expected for a free radical with one spin per molecule (C = 3/8 emu*K/mol); in Figure 7b we use the function $n = (8/3)*(\chi - \chi_0)*T$ to obtain the fraction of effective Curie spins per molecule (n) as a function of temperature (T). The plot shows that, in the solid state, **20** behaves as a free radical with ∼0.69 spins per molecule; thus, only about two out of every three available spins are magnetically active. We carried out a second set of magnetic susceptibility measurements on a different batch of **20** and obtained essentially identical results.

The results indicate that the paramagnetism in **20** is partially quenched, possibly because of the presence of the partial π-dimers. We note that the separation between the mean planes of the partial π-dimers decreases from 3.46 Å at $T = 293$ K to 3.39 Å at $T \approx 100$ K, and this change is expected to significantly increase the strength of the interaction between these two units and may play a role in the reduction of the Curie spin count. Below 50 K, the fraction of unpaired spins further decreases, which is to be expected in the case of a weak antiferromagnetic interaction where the population of the low spin ground state increases at low temperatures.

The single-crystal electrical conductivity of **20** as a function of temperature was measured in a four-probe configuration with in-line contacts, and the results are shown in Figure 8. The value of the room-temperature conductivity is $\sigma_{RT} = 2.4 \times 10^{-6}$ S/cm, and the data show semiconducting temperature dependence with activation energy of $\Delta = 0.37$ eV.

Optical Measurement of 20. To obtain further information on the electronic structure, we measured the transmission spectra of single crystal of **20**, and the results are presented in Figure 9. Transmission measurement is possible because of the needlelike morphology of the crystals, some of which are quite thin and are suitable for transmission measurement. The absorptions in the mid-IR, between 650 and 3000 cm^{-1}, are due to the molecular vibrations of the radical **20**. This optical energy gap E_g is comparable to that of the spiro-biphenalenyl boron radicals reported previously.[20,23,26]

Band Electronic Structure of 20. We carried out extended Hückel theory (EHT) band structure calculations[38] on the crystal structure of **20**. Such calculations have been very useful in understanding the electronic structure of organic molecular superconductor[39,40] and thin-film field effect transistors,[41] but cannot be expected to provide a complete picture of the electronic structure in situations where the tight-binding approximation is not applicable.[20]

The results are shown in Figure 10 for the calculation carried out on the reciprocal space lattice directions found in the X-ray crystal structure, whereas in Figure 11 the calculation was carried out along the diagonal directions ($^1/_2$ 0 0), (0 $^1/_2$ 0), (0 0 $^1/_2$), and ($^1/_2$ $^1/_2$ $^1/_2$).

The 12 bands shown in the figures are derived from the three LUMOs of $\mathbf{20}^+$, for each of the four molecules of **20** in the unit cell. Alternatively, they can be viewed as arising from the nonbonding molecular orbitals, of each of the 12 phenalenyl units in the unit cell. In the band picture, these 12 orbitals now accommodate a total of four electrons, leading to a one-sixth-filled band complex.

The maximum band dispersions found are 0.03 eV (a*), 0.02 eV (b*), and 0.02 eV (c*), whereas the maximum band dispersions along diagonal directions are 0.03 eV ($^1/_2$ 0 0), 0.03 eV (0 $^1/_2$ 0), 0.02 eV (0 0 $^1/_2$), and 0.02 eV ($^1/_2$ $^1/_2$ $^1/_2$); the extremely low band dispersions undoubtedly contribute to the low conductivity of the compound.

Conclusion

The first member of a new family of tris(1,9-disubstituted phenalenyl)silicon neutral radical conductors based on the O,N-ligand system has been synthesized and characterized, and the solid-state properties have been investigated. In the solid state, this radical neither remains strictly monomeric nor does it form isolated σ- or full π-dimers, and the crystal structure shows that this radical packs in a weak partial π-dimer structure. Magnetic

(38) Hofmann, R. *Solids and Surfaces;* VCH: New York, 1988.
(39) Haddon, R. C.; Ramirez, A. P.; Glarum, S. H. *Adv. Mater.* **1994**, *6*, 316−322.
(40) Williams, J. M.; Ferraro, J. R.; Thorn, R. J.; Carlson, K. D.; Geiser, U.; Wang, H. H.; Kini, A. M.; Whangbo, M.-H. *Organic Superconductors (Including Fullerenes): Synthesis, Structure, Properties, and Theory;* Prentice Hall: Englewood Cliffs, NJ, 1992.
(41) Haddon, R. C.; Siegrist, T.; Fleming, R. M.; Bridenbaugh, P. M.; Laudise, R. A. *J. Mater. Chem.* **1995**, *5*, 1719−1724.

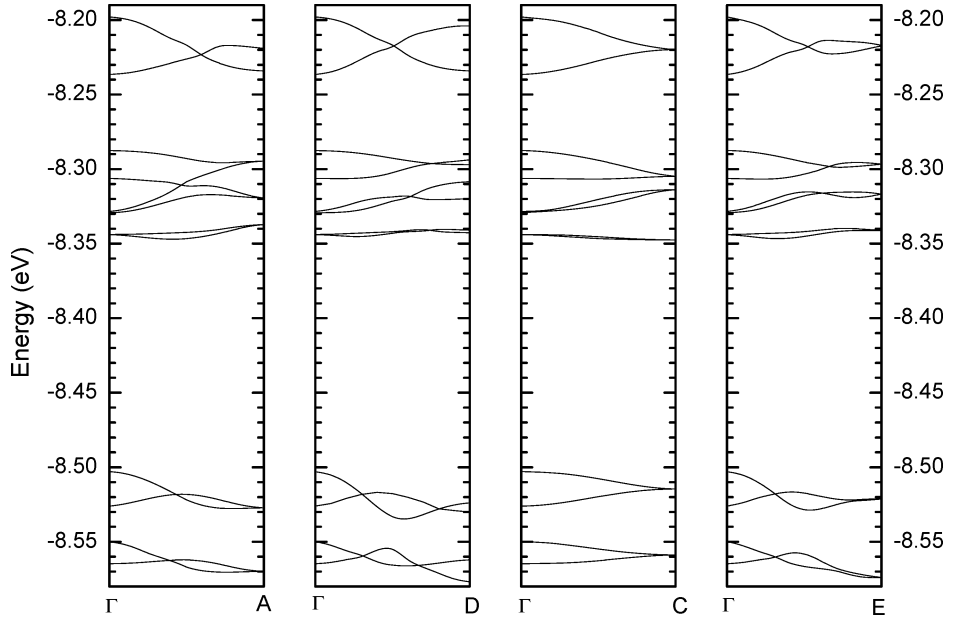

Figure 11. EHT band structure calculated for the experimental structure of crystalline **20** along diagonal directions, ($^1/_2$ 0 0), (0 $^1/_2$ 0), (0 0 $^1/_2$), and ($^1/_2$ $^1/_2$ $^1/_2$).

susceptibility measurements support the idea that the compound exists as an isolated free radical, but the reduced Curie spin count indicates the contribution of an antiferromagnetic interaction between the molecules in the solid state. The weak antiferromagnetic coupling observed in the magnetic susceptibility and the weak π-interactions in the solid-state structure are consistent with the low conductivity of the radical. The disproportionation energy, which largely determines the on-site Coulombic correlation energy in the solid state, is very similar to that of the spiro-bis(1,9-disubstituted phenalenyl)boron neutral radicals based on N,O- and N,N-ligand systems reported previously, and this is reflected in the measured conductivity. The conductivity of the solid is largely determined by the molecular packing; this radical shows weak intermolecular interactions through partial π-dimer formation and the absence of obvious conducting pathways in the crystal lattice. The crystallization of **20**, and the properties reported herein, suggests that a large class of trisphenalenyl radicals is now available for investigation, and if they can be crystallized (without σ- or π-dimerization), it should be possible to lower the disproportionation energies, increase the bandwidths, and obtain intrinsic molecular metals and superconductors.

Experimental Section

General Procedures and Starting Materials. Silicon tetrachloride (Aldrich), sodium tetraphenylborate (Aldrich), and cobaltocene (Strem) were all commercial products and were used as received. 9-*N*-Ethylamino-1-oxo-phenalene was synthesized according to literature procedures.[21] 1,2-Dichloroethane was distilled from CaH_2 just before use. Acetonitrile was distilled from P_2O_5 and then redistilled from CaH_2 immediately before use. Melting points were uncorrected. Infrared spectra were recorded on a Nicolet Nexus 670 FT-IR spectrometer at 2 cm^{-1} resolution. Mass spectra (MALDI) were run on a Voyager-DE STR BioSpectrometry Workstation mass spectrometer. Elemental analyses were performed by the Microanalysis Laboratory, University of Illinois, Urbana, IL.

Preparation of Tris(9-*N*-ethylamino-1-oxo-phenalene)silicon Chloride (20^+Cl^-). 9-*E*-Ethylamino-1-oxo-phenalene (1.0 g, 4.48 mmol) and triethylamine (0.63 mL, 4.5 mmol) in 1,2-dichloroethane (60 mL) were treated with silicon tetrachloride in dichloromethane (1.5 mL, 1.5 mmol) under argon, and the mixture was refluxed overnight at 70 °C. The yellow solid was isolated by filtration (1.0 g, 91%). MS (MALDI): *m*/*z* 694. The materials were taken to the next step without any further purification.

Preparation of Tris(9-*N*-ethylamino-1-oxo-phenalene)silicon Tetraphenyl Borate ($20^+BPh_4^-$). A solution of 0.58 g (1.72 mmol) of $NaBPh_4$ in 10 mL of methanol was added to a solution of $\mathbf{20}^+Cl^-$ (1.24 g, 1.69 mmol) in 20 mL of methanol. A yellow precipitate formed immediately. After being stirred for 15 min, the yellow solid was collected by filtration. The material so obtained was further purified by double recrystallization from acetonitrile to afford $\mathbf{20}^+BPh_4^-$ as yellow crystals: yield 0.49 g (29%); mp 156 °C. MS (MALDI): *m*/*z* 694. IR (4000−600 cm^{-1}): 2984 (w), 2869 (w), 1627 (s), 1578 (s), 1506 (s), 1469 (m), 1430 (w), 1361 (w), 1341 (m), 1292 (m), 1269 (m), 1246 (m), 1192 (m), 1166 (w), 1133 (m), 1079 (w), 963 (s), 934 (s), 916 (s), 844 (s), 795 (w), 747 (m), 734 (m), 703 (s), 685 (m). Anal. Calcd for $C_{69}H_{56}N_3O_3SiB0.5CH_3CN$: C, 81.26; H, 5.60; N, 4.74. Found: C, 80.42; H, 5.43; N, 4.34.

Crystallization of Tris(9-*N*-ethylamino-1-oxo-phenalene)silicon (20). A solution of 50 mg of $\mathbf{20}^+BPh_4^-$ in 20 mL of dry acetonitrile was placed in a sample vial inside a drybox, and 10 mg Cp_2Co was dissolved in 10 mL of dry acetonitrile in the other container. The cobaltocene solution was added very slowly into the BPh_4 salt solution by using a pipet. The sample vial was capped tightly and sealed with Parafilm and was removed from the drybox. The crystals started forming overnight. After sitting in the dark for 5 days, the container yielded 21 mg (61%) of black shining needles. Mp 95 °C (decomposed). IR (ATR, 4000−650 cm^{-1}): 3007 (w), 2920 (w), 1627 (s), 1581 (s), 1512 (s), 1466 (m), 1433 (m), 1361 (w), 1337 (m), 1320 (w), 1289 (s), 1243 (m), 1224 (w), 1186 (m), 1164 (w), 1133 (w), 1087 (w), 1051 (w), 962 (s), 936 (s), 917 (s), 840 (s), 824 (m), 802 (m), 752 (m), 677 (m). Anal. Calcd for $C_{45}H_{36}N_3O_3Si$: C, 77.78; H, 5.22; N, 6.05. Found: C, 76.32; H, 5.11; N, 6.85.

Cyclic Voltammetry. Cyclic voltammetric measurement was performed using a PINE Bipotentiostat, model AFCC1BP1, with scan rates of 100 mV/s on solutions ($<10^{-3}$ M) of $\mathbf{20}^+BPh_4^-$ in oxygen-free acetonitrile (distilled from CaH_2) containing 0.1 M tetra-*n*-butylammonium hexafluorophosphate. Potentials were scanned with respect to the saturated calomel as reference electrode in a single-compartment

cell fitted with Pt electrodes and reference to the Fc/Fc^+ couple of ferrocene at 0.38 V vs SCE.

EPR Spectra. The EPR spectra were recorded at ambient temperature using a Bruker EMX spectrometer on crystalline samples of **20**.

X-ray Crystallography. Data were collected on a Bruker SMART 1000 platform-CCD X-ray diffractometer system (Mo radiation, $\lambda =$ 0.71073 Å, 50 KV/40 mA power). The crystals were coated with paratone oil and mounted on glass fiber. The crystallographic parameters and the unit cell dimensions are summarized in Table 1. Absorption corrections were applied to the raw intensity data using the SADABS program in the SAINTPLUS software package.[42] The Bruker SHELX-TL (version 6.10) software package[43] was used for phase determination and structure refinement. Atomic coordinates, isotropic, and anisotropic displacement parameters of all the non-hydrogen atoms were refined by means of a full matrix least-square procedure on F^2. All H atoms were included in the refinement in calculated positions riding on the atoms to which they were attached. Full details, including bond lengths and bond angles, are given in the Supporting Information.

Magnetic Susceptibility Measurements. Magnetic susceptibility measurements on **20** were performed over the temperature range 10−300 K on a George Associates Faraday balance operating at 0.5 T. The system was calibrated using Al and Pt NIST standards.

Conductivity Measurements. The single-crystal conductivity (σ) of **20** was measured in a four-probe configuration using in-line contacts that were attached with silver paint. The needlelike crystal was freely positioned on a sapphire substrate, and the electrical connections between the silver paint contacts on the crystal and the indium pads on the substrate were made by thin, flexible 25-μm-diameter silver wires to relieve mechanical stress during thermal cycling of the crystal. The temperature dependence of the conductivity was measured in the range 330−160 K using a custom-made helium variable-temperature probe with a Lake Shore 340 temperature controller driven by LabVIEW software. A Keithley 236 unit was used as a voltage source and current meter, and two 6517A Keithley electrometers were used to measure the voltage drop between the potential leads in a four-probe configuration.

Single-Crystal IR and UV−Vis Transmission Spectroscopy. The infrared transmission measurements were carried out on an FT-IR Nicolet Nexus 670 ESP spectrometer integrated with a Continuum Thermo-Nicolet FT-IR microscope.

Band Structure Calculations. The band structure calculations made use of a modified version of the EHT band structure program supplied by M. H. Whangbo. The parameter set was chosen to provide a reasonably consistent picture of bonding in heterocyclic organic compounds.[41,44]

Acknowledgment. This work was supported by the Office of Basic Energy Sciences, Department of Energy, under Grant DE-FG02-04ER46138.

Supporting Information Available: EPR spectrum of **20**, ORTEP diagram of $\mathbf{20}^+BPh_4^-$, tables of crystallographic and structural refinement data, atomic coordinates, bond lengths, bond angles, and anisotropic thermal parameters, tables of bond lengths for standard deviation calculation, CIF files of structures **20** and $\mathbf{20}^+BPh_4^-$, and calculation of diamagnetic correction for the magnetic fitting. This material is available free of charge via the Internet at http://pubs.acs.org.

JA077771O

(42) *SAINTPLUS Software Reference Manual*, version 5.02; Bruker Analytical X-Ray System, Inc: Madison, WI, 1997−1998.
(43) *SHELXTL Software Reference Manual*, version 6.10; Bruker Analytical X-Ray System, Inc.: Madison, WI, 2000.
(44) Cordes, A. W.; Haddon, R. C.; Oakley, R. T.; Schneemeyer, L. F.; Waszczak, J. V.; Young, K. M.; Zimmerman, N. M. *J. Am. Chem. Soc.* **1991**, *113*, 582−588.